Surfactant-Induced Modification of Dopants Reactivity in Sol−Gel Matrixes

Claudio Rottman,† Gideon Grader,‡ Yoram De Hazan,‡ Sharona Melchior,‡ and David Avnir*,†

Institute of Chemistry, The Hebrew University of Jerusalem, Jerusalem 91904, Israel, and Faculty of Chemical Engineering, Technion, Haifa 32000, Israel

Received April 20, 1999

Abstract: Organically and bio-organically doped sol−gel materials have attracted much attention due to their ability to reproduce solution molecular activities within the ceramic environment. We take now this methodology one step forward and explore conditions under which the dopant properties can be modified by the matrix. Specifically we report that the co-entrapment of the surfactant cetyltrimethylammonium bromide (CTAB, the modifier) at low concentrations, with an extensive series of pH indicators representing several key molecular families (the primary dopant) within tetramethoxysilane (TMOS)-derived silica sol−gel matrixes, greatly modifies the indicating performance of the primary dopant. Thus, very large pK_i shifts of up to 3−4 orders of magnitude obtained upon the co-entrapment cause methyl orange (MO) to become an indicator for higher acidities and phenolphthalein for higher basicities, compared to their solution behavior. In another example, the ΔpK_i between the two indicating transitions of alizarin increased from ∼4.5 pH units in solution to ∼10.5 pH units (!) in the glass, transforming it into an indicator for both the high acidic and high basic pH ranges. In yet another example, the two indicating transitions of phenol red were shifted to a more acidic pH range, pushing the tail of the more acidic titration branch into the *negative* pH values range. These and other effects were found to be more pronounced by the co-entrapment than by the use of CTAB solutions or of sol−gel matrixes without CTAB, pointing to a synergetic effect between the surfactant and the silica cage. The indicators also proved highly sensitive in revealing the properties of the local environment created by the surfactant. Thus, the indicator molecules were shown to migrate and reorient within the hydrophobic and the hydrophilic regions of micellar environment, according to their acquired charge upon pH changes. The concentration-dependent and humidity-dependent surfactant aggregation processes within the silica cage were probed with MO, and the results were compared with the behavior of entrapped MO in sol−gel matrixes of varying hydrophobicities, obtained by the copolymerization of $CH_3Si(OCH_3)_3$ with TMOS at various ratios, with and without CTAB. Of practical importance have been the observations that the dopant/surfactant co-entrapment greatly improves the leaching profiles: half-lives, ranging from several months to several years, were found for MO and methyl red; and using SAXS, surface area and porosity measurements, it was shown that CTAB can be used to stabilize the microscopic structure of the material upon heat-drying. This provides a potential solution to the problem of continuing structural changes, which take place with sol−gel materials long after the completion of their synthesis.

1. Background

Direct entrapment of organic and bio-organic molecules within oxide sol−gel materials[1,2] is moving fast from basic science research to useful products. Examples include the 1 million TV sets sold annually by Toshiba, the screens of which are coated with a silica/zirconia sol−gel thin films, doped with indigo dyes;[3a] the organically doped sol−gel coated glassware sold by Spiegelau;[3b] and the sol−gel entrapped lipase sold by Fluka.[3c] Intensive R&D efforts toward many other products are strongly going on both in major industries and in many start-up companies. While dopants have been used successfully for tailoring the functionality of sol−gel-derived materials, one should take into account also the conjugated effect: Exposing the dopant to the cage environment may be used to influence its properties. Modifying the functionality by affecting the dopant properties through entrapment is an approach that is yet to be fully explored and is the topic of this report. We show here that this approach carries a potential that is at least as wide as the straightforward entrapment.

(1) Some recent publications in this journal: (a) Kanti Das, T.; Khan, I.; Rousseau, D. L.; Friedman, J. M. *J. Am. Chem. Soc.* **1998**, *120*, 10268. (b) Jain, T. K.; Roy, I.; De, T. K.; Maitra, A. *J. Am. Chem. Soc.* **1998**, *120*, 11092. (c) Greaves, D. M.; Rotello, V. M. *J. Am. Chem. Soc.* **1997**, *119*, 10268. (d) Chen, Q.; Kenausis, G. L.; Heller, A. *J. Am. Chem. Soc.* **1998**, *120*, 4582. (e) Rao, M. S.; Dave, B. C. *J. Am. Chem. Soc.* **1998**, *120*, 13270.

(2) For recent reviews see: (a) Avnir, D.; Klein, L. C.; Levy, D.; Schubert, U.; Wojcik, A. B. In *The Chemistry of Organosilicon Compounds*; Apeloig, Y., Rappoport, Z., Eds.; Wiley & Sons: Chichester, U.K., 1998; Vol. 2, Chapter 40, p 2317. (b) Blum, J.; Avnir, D.; Schumann, H. *CHEMTECH* **1999**, *29*, 32. Some additional recent publications from our research group: (c) Ramanathan, K.; Avnir, D.; Modestov, A.; Lev, O. *Chem. Mater.* **1997**, *9*, 2533. (d) Shabat, D.; Grynszpan, F.; Saphier, S.; Turniansky, A.; Avnir, D.; Keinan, E. *Chem. Mater.* **1997**, *9*, 2258. (e) Altstein, M.; Bronshtein, A.; Aharonson, N.; Avnir, D.; Turniansky, A. *Chem. Mater.* **1997**, *9*, 2632. (f) Ben-David, O.; Shafir, E.; Gilath, I.; Prior, Y.; Avnir, D. *Chem. Mater.* **1997**, *9*, 2255. (g) Schumann, H.; Hasan, M.; Gelman, F.; Avnir, D.; Blum, J. *Inorg. Chim. Acta* **1998**, *280*, 21. (h) Gelman, F.; Avnir, D.; Schumann, H.; Blum, J. *J. Mol. Catal.* **1999**, in press. (i) Shacham, R.; Avnir, D.; Mandler, D. *Adv. Mater.* **1999**, *11*, 1544.

(3) Itou, T.; Matsuda, H. *Key Eng. Mater.* **1998**, *67*, 150. (b) Schottner, G.; Kron, J.; Deichmann, K. J. *J. Sol-Gel Sci. Technol.* **1998**, *13*, 183. (c) Aldrich, Fluka, Sigma, and Supelco *Chiral Products* Catalog 1997; p 250. See also ref 11.

10.1021/ja991269p CCC: $18.00
Published on Web 09/03/1999

In general, the properties of the dopants are dictated by the interfacial moieties of the ceramic material.[4] In the case of porous silica xerogels these moieties comprise of all types of silanols (isolated, geminal, vicinal),[5] siloxane bridges, residual water and alcohol molecules, and leftover of unhydrolyzed alkoxy groups and acid/base catalysts molecules.[6] This immediate environment of the dopant may affect and modify its optical properties, its chemical performance and its stability, and hence the interest and the potential in tailoring cage properties which are different than the native ones. One major route has been to polymerize or copolymerize monomers which carry a nonhydrolizable residue, resulting in what has become known as Ormosils.[7,8] The residue, R, can induce hydrophobicity, aprotic polarity, acidity/basicity changes, and so on. Since R is nonpolymerizable, its local concentration within the cage is high. An early example from our laboratory that describes the successful application of this approach was the preparation of reversible photochromic sol−gel materials by the entrapment of spiropyranes in a hydrophobically modified cage.[9] Interestingly, only by this cage modification was it possible to retain the reversibility in the photochromism of the entrapped molecule. Some more recent examples for the successful tailoring of properties by this approach are the composite sol−gel/carbon electrodes,[10] the enhancement of the activity of lipase by its entrapment in alkylated silica sol−gel matrixes,[3c,11] and the sensing of alcohols by the entrapment of the solvatochromic dye $E_T(30)$ in methylated silica sol−gel.[12]

The second methodology for affecting cage properties, which is at the focus of this report, is the co-entrapment of surface-active agents (SAAs). Our preliminary interest in the study of added SAAs has been their use as cracking preventing agents for sol−gel monoliths along their drying or wetting.[13,14] Recent elegant studies of a dopant−surfactant co-entrapment include the dopant photophysical studies of Lianos et al.[15] and of Ogawa et al.[16] It is also relevant in this context to recall that surfactants, at either low[17] or very high concentrations[18] (several hundred times higher than the concentration used in this report) proved to be useful templating agents for sol−gel-derived materials.[19]

Scheme 1[a]

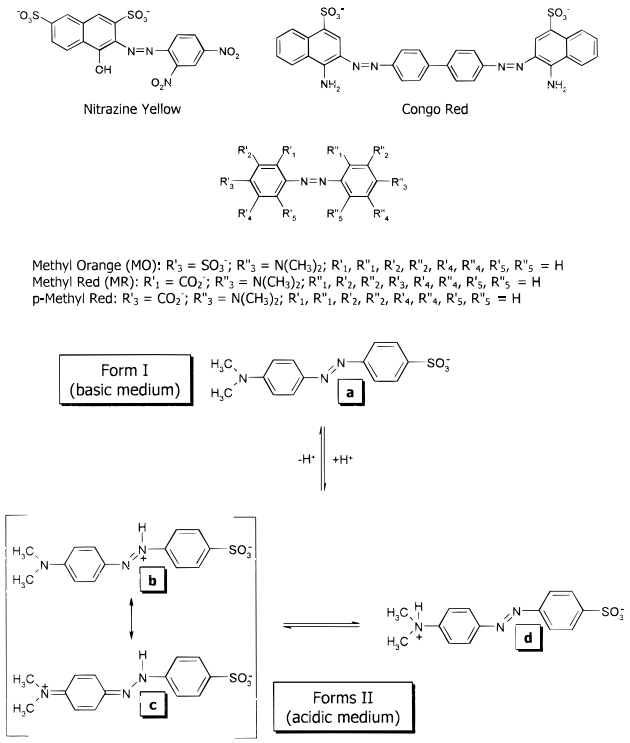

[a] Top: structures of the azo indicators used in this study. Bottom: representative structural changes (shown for methyl orange, MO), causing migration of the molecule between the hydrophobic and hydrophilic zones of the entrapped CTAB aggregates.

The specific systems we have studied comprise a long series of pH indicators representing several molecular families, co-entrapped with cetyltrimethylammoniumbromide (CTAB) within sol−gel tetramethoxysilane (TMOS)-derived silica matrixes. Since doped sol−gel glasses for sensors preparation are among the prime applications of these materials,[20] our motivation for this co-entrapment has been not only the basic science aspect of rational control of dopant properties but also the opening of a new methodology for the design of properties of sensing and reactivity. In doing so, we were also able to probe the chemical nature of the immediate environment of the dopant molecule, namely, to get some insight on the structure of low concentration entrapped surfactants. We recall that a central feature of sol−gel entrapment has been that the doping breaks down dimers and other aggregates,[21] and so a question raised has been whether the surfactant molecules are entrapped as isolated molecules or as aggregates, and if so, do the aggregates retain distinct hydrophobic and hydrophilic regions. As already indicated in the Abstract, the power of codoping to alter significantly the properties of the primary dopant has been demonstrated; some insight on the conditions under which low concentrations of surfactants are aggregated within the silica matrix has been gained. Details follow in Sections 3 and 4.

2. Experimental Details

2.1. Chemicals. Cetyltrimethylammoniumbromide (CTAB) was from Fluka. $Si(OCH_3)_4$ and $CH_3Si(OCH_3)_3$ were from Aldrich.

2.1.1. Families of Entrapped Indicators. *Azo indicators* (for structures, see Scheme 1): Methyl orange (MO) (BDH), methyl red

(4) K. Dunn, B.; Zink, J. *Chem. Mater.* **1997**, *9*, 2280.
(5) Li, Z.; Rutan, S. C. *Anal. Chim. Acta* **1995**, *312*, 127 and references therein.
(6) Brinker, J. C.; Scherer, G. W. In *Sol−Gel Science: The Physics and Chemistry of Sol−Gel Processing*; Academic Press: San Diego, CA, 1990.
(7) Hüsing, N.; Schubert, U.; Misof, K.; Fratzl, P. *Chem. Mater.* **1998**, *10*, 3024.
(8) Mark, J. E. *Heterog. Chem. Rev.* **1996**, *3*, 307.
(9) Levy, D.; Einhorn, S.; Avnir, D. *J. Non-Cryst. Solids* **1989**, *113*, 137.
(10) Tsionsky, M.; Gun, G.; Glezer, V.; Lev, O. *Anal. Chem.* **1994**, *66*, 1747.
(11) Reetz, M. T.; Zonta, A.; Simpelkamp, J. *Angew. Chem., Int. Ed. Engl.* **1995**, *34*, 301.
(12) Rottman, C.; Grader, G. S.; De Hazan, Y.; Avnir, D. *Langmuir* **1996**, *12*, 5505.
(13) Rottman, C.; Ottolenghi, M.; Zusman, R.; Lev, O.; Smith, M.; Gong, G.; Kagan, M. L.; Avnir, D. *Mater. Lett.* **1992**, *13*, 293. (b) Rottman, C.; Turniansky, A.; Avnir, D. *J. Sol-Gel Sci. Technol.* **1998**, *13*, 17.
(14) Kraus, S. C.; Czolk, R.; Reichert, J.; Ache, H. J. *Sens. Actuators, B* **1993**, *15−16*, 199.
(15) Ferrer, M.; Lianos, P. *Langmuir* **1996**, *12*, 5620. (b) Ferrer, M.; Bekiari, V.; Lianos, P. *Chem. Mater.* **1997**, *9*, 2652. (c) Bekiari, V.; Ferrer, M.; Lianos, P. *J. Phys. Chem.* **1999**, in press.
(16) Ogawa, M. *Langmuir* **1995**, *11*, 4639.
(17) Murakata, T.; Sato, S.; Ohgawara, T.; Watanabe, T.; Suzuki, T. *J. Mater. Chem.* **1992**, *27*, 1567.
(18) Goltner, C. G.; Antonietti, M. *Adv. Mater.* **1997**, *9*, 431.
(19) Sellinger, A.; Weiss, P. M.; Nguyen, A.; Lu, Y.; Assink, R. A.; Gong, W.; Brinker, C. J. *Nature* **1998**, *394*, 256. (b) Tanev, P. T.; Chibwe, M.; Pinnavaia, T. J. *Nature* **1994**, *368*, 317. (c) Ramsay, J. *Curr. Opin. Colloid Interface Sci.* **1996**, *1*, 208. (d) Raman, K. N.; Anderson, M. T.; Brinker, C. J. *Chem. Mater.* **1996**, *8*, 1682. (e) Tolbert, S. H.; Firouzi, A.; Stucky, G. D.; Chmelka, B. F. *Science* **1997**, *278*, 264. (f) Zhang, W.; Pauly, T. R.; Pannavaia, J. T. *Chem. Mater.* **1997**, *9*, 2491.
(20) Wolfbeis, O. S.; Reisfeld, R.; Oehme, I. In *Sol Gel and Chemical Sensors*; Springer: Berlin, Germany, 1996.
(21) Innocenzi, P.; Kozuka, H.; Yoko, T. *J. Non-Cryst. Solids* **1996**, *201*, 26. (b) Avnir, D.; Levy, D.; Reisfeld, R. *J. Phys. Chem.* **1984**, *88*, 5954.

Scheme 2[a]

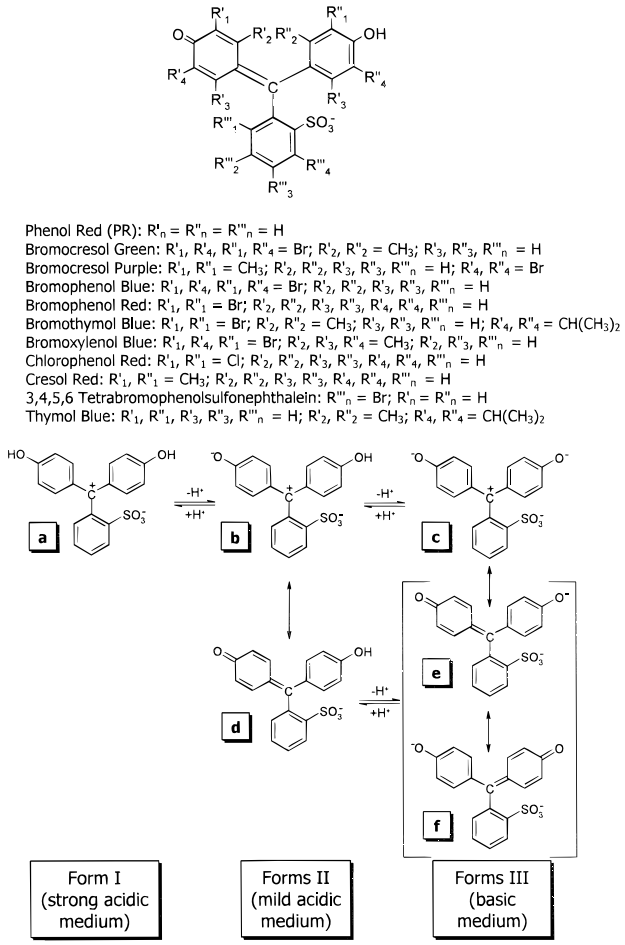

[a] Top: structures of the sulfonephthaleins used in this study. Bottom: representative structural changes shown for phenol red (PR).

(MR) (Aldrich), *p*-(*p*-dimethylaminophenylazo)benzoic acid sodium salt (pMR) (Kodak), Congo red (Aldrich), and nitrazine yellow (Aldrich). *Sulfonephthalein indicators* (Scheme 2): Bromocresol green sodium salt (Aldrich), bromocresol purple sodium salt (Aldrich), bromophenol blue (Aldrich), bromophenol red (Fluka), bromothymol blue (Aldrich), bromoxylenol blue (Aldrich), chlorophenol red sodium salt (Aldrich), cresol red sodium salt (Aldrich), phenol red sodium salt (PR) (Aldrich), thymol blue sodium salt (Aldrich), and 3,4,5,6-tetrabromophenolsulfonephthalein (Aldrich). *Phthalein indicators* (Scheme 3): α-naphtholphthalein (Fluka), phenolphthalein (P) (Aldrich), and thymolphthalein (Aldrich). Alizarin (AL, for structure see Scheme 4) (Merck).

2.2. Entrapment Procedures. 2.2.1. The System SiO_2/CTAB/pH Indicator. The following mixture was prepared in a 20 mL flask: 2.5 mL of MeOH, 2.5 mL of TMOS, and 1.0 mL of an 8.2×10^{-2} M methanolic solution of CTAB (CTAB/Si molar ratio = 4.8×10^{-3}:1). The mixture was sonicated for 5 min, after which 2.3 mL of water (H_2O/Si molar ratio = 7.6:1) and 0.1 mL of a 0.02−0.1% (by weight) solution of the indicator in either water or MeOH (varying according to the nature of the indicator) were added. The final mixture was sonicated for 10 more minutes and poured into a Petri dish (60 mm in diameter, 20 mm high), covered, and left at room temperature for 5 days for the gelation and initial shrinkage. The wet gel was then dried for 2 days in an oven at 45−50 °C, during which the gel shrank further (approximately 70% from the starting volume), resulting in a transparent disk with typical dimensions of 26 mm in diameter and thickness of 2.5 mm.

2.2.2. The System SiO_2/CTAB/MO. The effects of the CTAB concentration were studied on MO with a series of glasses prepared as in 2.2.1, varying the molar ratio CTAB/Si from 0:1 to 4.8×10^{-3}:1.

2.2.3. The System MeTMOS/TMOS/MO. To provide proof for the reasoning of the effects of concentration changes of CTAB, it was

Scheme 3[a]

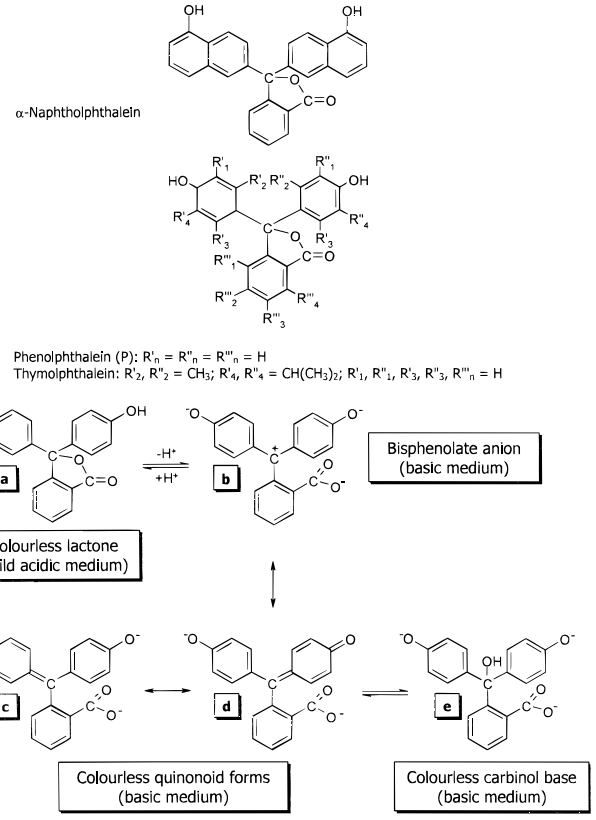

[a] Top: structures of the phthaleins used in this study. Bottom: representative structural changes, shown for phenolphthalein (P).

Scheme 4. The Structures of Alizarin (AL)

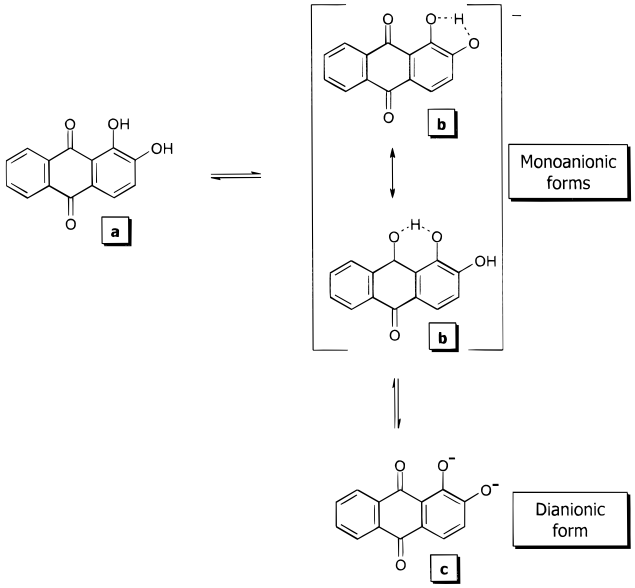

interesting to follow the effects of gradually blocking the acidic silanol groups with methyl groups. Thus, a high load of methyl groups would allow the entrapment of the methyl orange (MO) in its anionic form (Scheme 1) due to the lower acidity and higher hydrophobicity of the cage walls. For this purpose a series of Ormosil glasses varying the molar ratio MeTMOS/TMOS (MeTMOS = methyltrimethoxysilane) from 0.0:1.0 to 0.55:0.45 was prepared as in 2.2.1 but without added CTAB.

2.2.4. The System MeTMOS/TMOS/CTAB/MO. On the basis of the λ_{max} values of the absorbance spectra of the Ormosil series prepared in 2.2.3, we selected (see below the reasoning) the molar ratio

Table 1. Properties of the Indicators in Sol−Gel Glass and in Solution

indicator	pH indicating range		color change[c]	λ_{max} (nm)[a]		
	in glass	in solution[b]		in glass	in solution + CTAB	in solution
azo indicators						
congo red	0.0−2.0	3.0−5.2	B−R	586, 479	586, 479	580, 476
nitrazine yellow	4.9−6.4	6.0−7.2	Y−B	468, 598	468, 596	465, 588
methyl orange	0.0−2.0	2.9−4.6	R−Y	508, 428	510, 428	510, 466
methyl red	3.9−5.6	4.2−6.2	R−Y	522, 422	518, 418	518, 436
p-methyl red	0.2−1.8	1.0−3.0	RO−Y	506, 430	506, 430	510, 464
sulfonephthalein indicators						
bromocresol green	1.5−3.8	3.8−5.4	Y−B	414, 624	422, 626	445, 616
bromocresol purple	3.9−5.8	5.2−6.8	Y−Pu	418, 600	418, 600	434, 588
bromophenol blue	0.0−2.0	3.0−4.6	Y−B	424, 604	424, 604	438, 592
bromophenol red	3.8−5.8	5.2−6.8	Y−R	430, 582	428, 588	440, 574
bromothymol blue	5.3−7.0	6.0−7.6	Y−B	420, 624	420, 626	434, 616
bromoxylenol blue	4.8−6.6	6.0−7.6	Y−B	414, 624	412, 624	437, 614
chlorophenol red	3.8−5.8	4.8−6.4	Y−R	424, 582	422, 588	436, 574
cresol red	4.0−6.0	7.0−8.8	Y−R	420, 580	418, 584	434, 572
phenol red (ar)[d]	(−2.0)−1.2	0.0−2.0	OR−Y	516, 430	514, 422	506, 432
phenol red (br)[d]	5.0−7.0	6.8−8.2	Y−R	430, 564	422, 572	432, 558
3,4,5,6-tbpsp[e]	5.0−7.0	6.6−8.2	Y−P	434, 586	430, 588	436, 576
thymol blue (ar)[d]	(−2.0)−1.2	1.2−2.8	R−Y	556, 440	556, 440	546, 436
thymol blue (br)[d]	4.3−5.8	8.0−9.2	Y−B	440, 602	440, 606	436, 596
phthalein indicators						
α-naphtholphthalein	9.8−11.3	7.8−9.0	PBr−B	650	648	654
phenolphthalein	11.8−14.0	8.0−10.0	C−P	560	560	552
thymolphthalein	12.0−14.0	8.8−10.5	C−B	592	594	598
alizarin						
alizarin (ar)[d]	1.8−4.0	4.3−6.3	Y−R	428, 526	432, 526	422, 518
alizarin (br)[d]	13.0−14.0	9.4−12.0	R−V	526, 572	526, 572	518, 554
				(604)[f]	(618)[f]	(594)[f]

[a] Left value, acidic form; right value, basic form. [b] Reference 23. [c] Left color, acidic form; right color, basic form; B, blue; C, colorless; O, orange; OR, orange-red; P, pink; PBr, pinkish-brown; Pu, purple; R, red; RO, reddish-orange; V, violet; Y, yellow. [d] ar, acidic range; br, basic range. [e] 3,4,5,6-Tetrabromophenolsulfonephthalein. [f] Multiple λ_{max} peaks in the basic molecular form.

MeTMOS/TMOS = 0.3:0.7, which contains the basic form of MO. A series of these Ormosils with varying molar ratios of CTAB/Si in the range 0:1 to 4.8×10^{-3}:1 was prepared using the procedure described in 2.2.1.

2.2.5. Blank Systems. (i) MO and P were entrapped in pure silica according to procedure (2.2.1) but without added CTAB. (ii) Twelve nonbuffered solutions of MO and P (3.2×10^{-5}M) in aqueous 0.1% (by weight) CTAB (which is approximately the concentration of CTAB in the glass) at different pH values were prepared. The pH ranges were 0.01−2.70 for MO and 10.6−13.5 for P. (iii) Fifteen surfactant solutions of MO (3×10^{-5} M) at pH = 7.02 were prepared at varying CTAB concentrations from 0 to 6 mM, following reference 22.

2.2.6. Leaching tests were carried out by 3−4 washing cycles with ~50 mL of deionized water in which the selected piece of monolithic glass was shaken for about 30 min. Static leaching tests were carried out by placing the sol−gel glass (~8 × 10 × 1.5 mm) in 50 mL of water solution of the desired pH value.

2.3. pH-Indicating Performance. pH changes were affected with nonbuffered solutions. Maximum absorption values, λ_{max}, were determined by taking full spectra within the cell of a HP 8453 diode array spectrophotometer. Full titration curves were obtained from the changes in λ_{max}, after the sol−gel glass had been immersed in solutions of different pH values, and after equilibrium was reached (about 15 min after the glass immersion). Isosbestic points were determined by taking full spectra each 5−20 s (depending on the indicator).

2.4. SAXS, Surface Area, and Porosity Measurements. Small-angle X-ray scattering (SAXS) measurements were performed for selected samples of the series belonging to the system SiO_2/CTAB/MO (entrapment procedure 2.2.2). The samples were prepared by crushing the monoliths and placing the resulting powder into epoxy sealed 1.5 mm thin-walled capillaries. The SAXS profiles of this series of monoliths were measured before and after a drying process in which the monoliths were heated at 100 °C in a drying oven for 5 h. SAXS measurements were performed using Cu Ka radiation with a compact Kratky camera (Phillips PIN730 sealed tube generator) having a linear position sensitive detector system (Raytech). Sample to detector distance was 26.4 cm. Temperature was kept at 25 °C with a temperature-controlled sample holder (A. Paar Co.) during data accumulation. Slit smeared data was analytically desmeared by subtracting 1 from the Porod slope. Specific surface area and average pore sizes for this series were determined from nitrogen adsorption/desorption data using a Micromeritics ASAP 2000 instrument. BET surface areas and BJH porosities are reported.

(22) Gehlen, M. H.; Ferreira, M.; Neumann, M. G. *J. Photochem. Photobiol. A* **1995**, *87*, 55.

3. Results

3.1 The Effects of CTAB on the Properties of the Dopants.

3.1.1. Spectral Shifts and Indicating Range Shifts. In Table 1 are collected the observations made regarding the indicating ranges and the spectral characteristics of the various entrapped molecules in CTAB micellar aggregates within the SiO_2 sol−gel glass, along with comparison to solution values. It is seen that the indicating ranges of the entrapped azo and sulfonephthalein dyes are shifted to more acidic values, while the phthalein indicators are shifted to more basic values. We explain and rationalize this observation in the Discussion.

3.1.2. Isosbestic Points. Determination of isosbestic points within the porous glass is shown in Figure 1 for representative dyes. The sharp isosbestic points of MO and PR (Figure 1, parts a and b, respectively), which are similar to the sharpness in solution, attest to the homogeneous environment that the entrapped dyes experience. The molecules with two indicating ranges, thymol blue and phenol red (PR) (Scheme 2), revealed in their entrapped form two isosbestic points, as shown for example for PR (Figure 1b). (No isosbestic point is seen for P in the visible because the closed lactone (Scheme 3) absorbs only in the UV).

3.1.3. Titration Curves and pK_i. Typical titration curves in the SiO_2/CTAB glass are shown in Figure 2 for P and MO, for

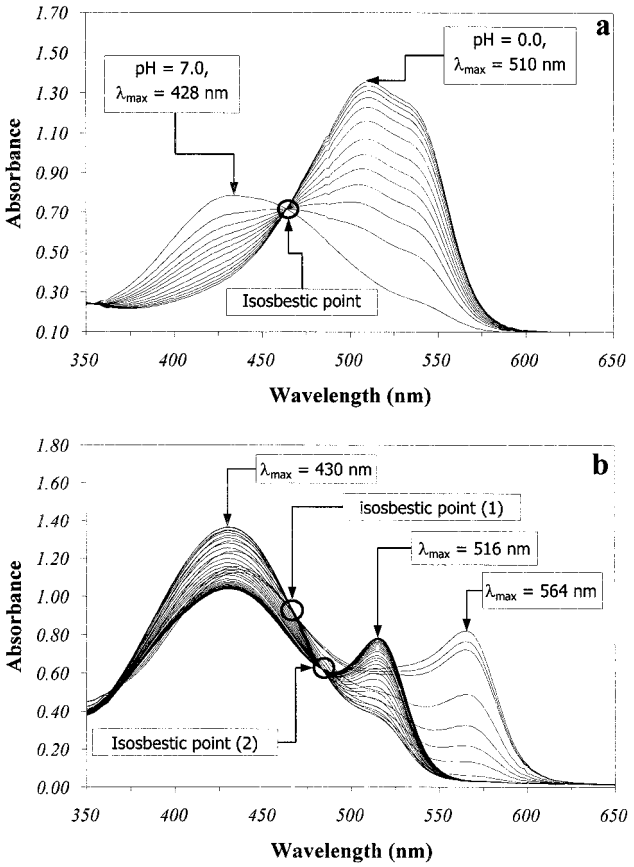

Figure 1. Representative isosbestic point behavior of entrapped indicators: (a) an azo indicator (methyl orange) and (b) a sulfonephthalein indicator (phenol red).

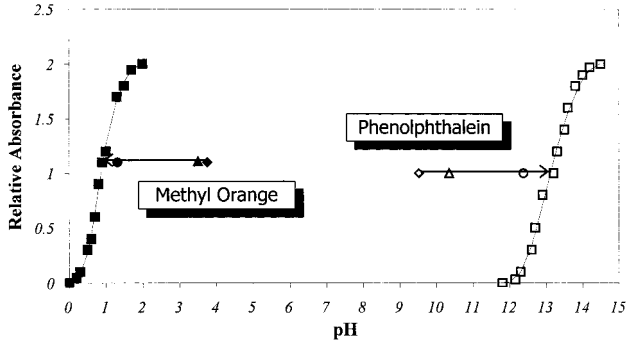

Figure 2. The titration curves of methyl orange (■) and phenolphthalein (□) in the CTAB/sol−gel glass. The pK_i shifts are shown as well: Aqueous nonbuffered solution (◆, $\Delta pK_i = 2.85$; ◇, $\Delta pK_i = 3.68$), sol−gel glass without CTAB (▲, $\Delta pK_i = 2.60$; △, $\Delta pK_i = 2.85$), and aqueous CTAB solution (●, $\Delta pK_i = 0.38$; ○, $\Delta pK_i = 0.82$). Note the large pK_i shifts, the opposite direction of the shifts for the two indicators, and the synergetic effects of CTAB combined with that of the silica cage.

which pK_i values of 13.0 and 0.9 were obtained, respectively. These pK_i values represent very large shifts (3 and 4 orders of magnitude for MO and P, respectively) compared to aqueous solution (Figure 2). Interestingly, these shifts are larger than those obtained by either dissolving in CTAB aqueous solution or entrapment in pure sol−gel silica glass without CTAB (Figure 2). We return to this effect in the Discussion. The shifts for MO and P are in *opposite* directions: in sol−gel, MO becomes an indicator for highly acidic solutions and P becomes an indicator for highly basic solutions; this, as we shall see in the Discussion, conforms with the existence of micellar-like CTAB

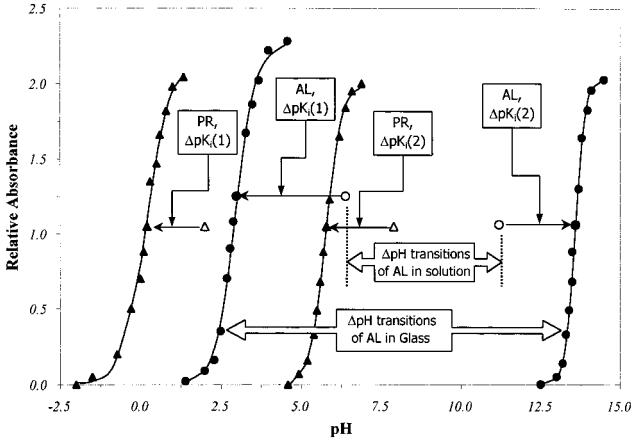

Figure 3. Phenol red (PR) and alizarin (AL) have each two indicating transitions (Schemes 1and 4). For PR (▲) the pK_is of the two indicating regions in CTAB/sol−gel glass are 0.25 and 5.6 (vs 2.0 and 7.9 in aqueous nonbuffered solution (△)). For AL (●) the pK_is of the two indicating regions in CTAB/sol−gel glass are 2.7 and 13.5 (vs 6.4 and 11.2 in aqueous nonbuffered solution (○)). Note that the separation between the two indicating transitions of AL increases from ∼4.5 pH units in solution, to ∼10.5 pH units (!) in the glass, making it an indicator for both extreme acidic and basic conditions. Note also that the tail of the PR enters the range of *negative* pH values.

structures and with the different pH-dependent charge changes of the two indicators.

The titration curve behavior of indicators with two transitions at different pH values is shown in Figure 3 for entrapped PR and AL. Large pK_i shifts, compared to solution, are also observed here but with a special twist: the two transitions can be shifted either to the same direction, as for PR (and for thymol blue; see Table 1), or in opposite directions, as for AL. There are two interesting consequences to these shifts: first, the acidic pK_i shift of PR (and thymol blue also) pushes the tail of the curve to the *negative* pH values range, making it the most acidic sol−gel pH indicator we are aware of in this kind of matrix; and, second, the separation between the two transitions in AL increases by a factor of 1 million from ∼4.5 pH units to ∼10.5 pH units, transforming AL into a very interesting indicator for both high acidity and high basicity. As seen in Table 1, large shifts are generally typical for most indicators.

3.1.4. Stability and Response Time. The stability of the doped silica matrixes to repeated measurement cycles and the time needed to reach plateau readings upon pH changes were checked. It was found that, while under neutral and acidic environments, the matrix is very stable; under highly basic conditions degradation is apparent, which is probably due to the irreversible hydrolysis of siloxane bonds. Typical results are shown for MO and of P in Figure 4. For each point, equilibrium was assured by waiting either 15 or 30 min until plateau was reached, depending on whether the cycle steps were consist with a protonation−deprotonation process at high or low ion concentration (proton or hydroxyl), respectively. Following ref 4, we ascribe this difference to the specific immediate microenvironment around the indicator molecules, which is composed of pH-dependent moieties such as silanols: Faster responses are associated with the higher concentration change gradients between the outside environment and the effective pH within the cage, while slower responses reflect mild pH gradients. It should be mentioned here that, while these response times are typical for monoliths, fast response time is easily achieved by reducing the dimensions of the doped material.[24,25]

(23) Bishop E. *Indicators*; Pergamon Press: Oxford, U.K., 1972.

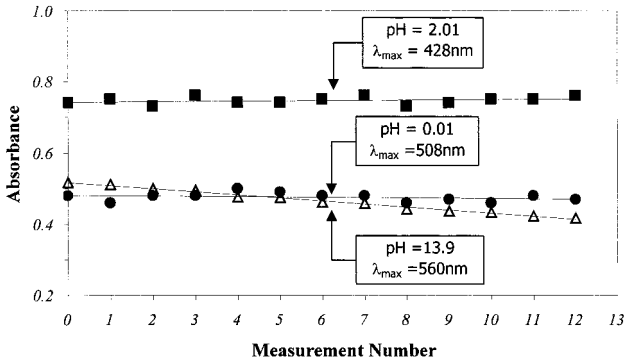

Figure 4. Reproducibility of 12 cycles of measurements for methyl orange (● and ■) and phenolphthalein (△).

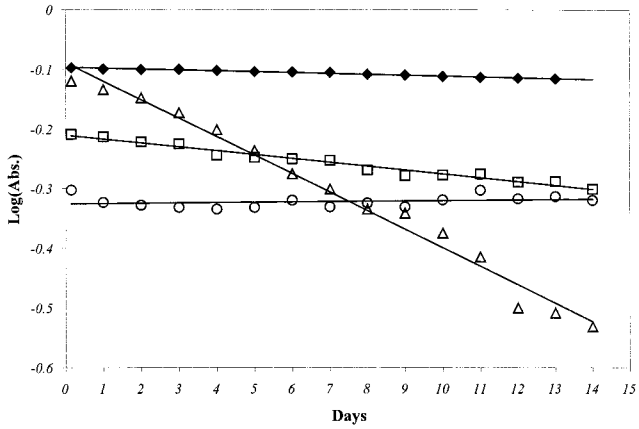

Figure 5. Leaching behavior of methyl orange (○, □, △) and methyl red (◆) co-entrapped in sol−gel with CTAB. The pseudo first-order half-lives are the following: (○) 3.5 years ± 8 months at neutral pH; (□) 3.5 months ± 10 days at pH 2.0; (△) 23 days ± 3 days at pH 0.0; and (◆) 1.5 years ± 2 months at pH 0.01.

Another tested aspect of stability was the rate of leaching, which provided some excellent results. We reproduce for the Discussion previous observations we made on the leaching behavior of MO[13a] and of MR,[13b] both in the system SiO_2/CTAB (Figure 5). Following Carturan et al.[26] and others,[27] we use a pseudo-first order analysis, from which the leaching half-life for MR is 1.5 years. MO shows similarly excellent stability for neutral conditions ($t_{1/2}$ = 3.5 years), good stability at pH = 2.0 ($t_{1/2}$ = 3.5 months), and slow leaching at the extreme pH = 0.0 ($t_{1/2}$ = 23 days; even this lifetime is sufficiently large disposable measurements applications).

3.2. Effects of Changes in CTAB Concentration. 3.2.1. As Probed by Methyl Orange. At the background, let us first recall the λ_{max} change in behavior of MO in water solution and in CTAB water solution,[22,28,29] from the longest to the shortest λ_{max} values. The reddest λ_{max} value of MO is obtained for its acidic zwitterionic structure (b−d in Scheme 1) at 510 nm. The basic anionic structure (*a* in Scheme 1) absorbs at λ_{max} = 466 nm (Figure 6 at zero CTAB concentration). In micellar solution at pH = 7.0 (Figure 6), the basic anionic structure within the hydrophobic micellar environment has its shifted λ_{max} value at

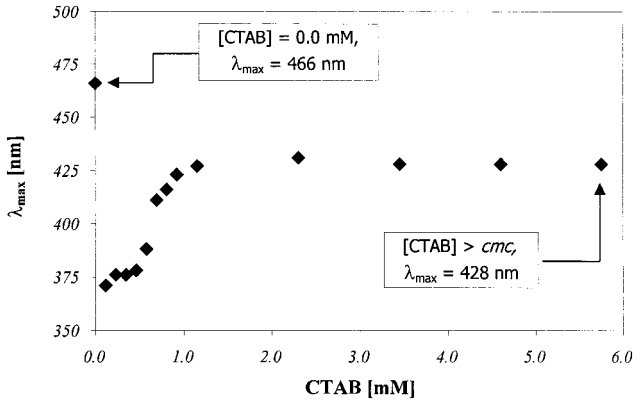

Figure 6. Spectral shifts of λ_{max} of methyl orange in aqueous CTAB solution (pH = 7.0) as a function of CTAB concentration.

428 nm (the plateau in Figure 6). Also shown in Figure 6 is the gradual build-up of the micelle, reaching a cmc at about 1 mM CTAB (0.9 mM in solution).[29] Finally, the bluest absorption is seen as the sharp drop in the λ_{max} from 466 nm at zero CTAB concentration to λ_{max} = 370 nm at very low CTAB concentration of 0.1 mM. This absorption, which apparently is due to ion-pairing and hydrophobic interactions between MO and CTAB (see Discussion), is then gradually red-shifted until the cmc is reached (Figure 6), following the transition from MO which interacts with CTAB pre-micelle aggregates, to the micelle itself. Having this picture in solution, let us now move on to three types of entrapped systems: MO in CTAB/silica; MO in methylated (Me) hydrophobic silica; and MO in CTAB/Me-silica.

The effects of changing the CTAB concentration from zero to beyond the *cmc* value on the λ_{max} of entrapped MO (Procedure 2.2.2) are shown in Figure 7. The dried glass (Figure 7a; 60 °C, 24 h) and the same glass after exposure to air humidity (Figure 7b) show a markedly different behavior, with the former reaching very short λ_{max} values of 355 nm (cf. Figure 6 and Discussion). It is also seen (Figure 7a) that the λ_{max} value at zero CTAB, namely, 466 nm, is practically the anionic form of MO; that is, hydrogen bonds between the MO molecules and the silanols at the interface of the pure dried silica are developed in a way which resembles the interaction with water. It is also seen that, following the sharp drop to 355 nm upon the addition of small amount of CTAB, there is then a gradual rise in λ_{max} to 375 nm, but it never reaches the λ_{max} value, which is indicative of the formation of a micellar structure (cf. Figure 6). The crucial role of adsorbed water for the formation of a micellar structure within the sol−gel matrix is then seen in Figure 7b, i.e., in the humidity-exposed glass: Here at the higher CTAB concentration, a λ_{max} = 428 nm is reached, exactly as in Figure 6. Notice also that, whereas in the dried glass at zero CTAB concentration the interface resembles, as indicated above, neutral water (λ_{max} of MO = 466 nm), a λ_{max} of 508 nm in the wet glass is that of the acidic zwitterionic form; it is corroborated that caged water molecules are needed in order to express the acidity of the silanols.[30]

3.2.2. As Probed by SAXS and Surface Area Measurements. The effects of CTAB on the matrix structure and on the response to drying (100 °C for 5 h) were also probed by SAXS and by surface area/porosity measurements. We begin with the former, for which six samples were prepared with the general composition SiO_2/CTAB/MO having different surfactant concentrations of 0.0, 0.2, 0.4, 0.8, 2.0, and 10.0 mM (see Experimental Procedure 2.2.2.). Figures 8 and 9 show the

(24) Lee, J. E.; Saavedra, S. S. *Anal. Chim. Acta* **1994**, *285*, 265.
(25) Butler, T. M.; MacCraith, B. D.; McDonagh, C. *J. Non-Cryst. Solids* **1998**, *224*, 249.
(26) Carturan, G.; Pagani, R.; Campostrini, R.; Ceccato, R. *J. Sol−Gel Sci. Technol.* **1997**, *8*, 1115.
(27) Lobnik, A.; Oehme, I.; Murkovic, I.; Wolfbeis, O. S. *Anal. Chim. Acta* **1998**, *367*, 159.
(28) Kunitake, T.; Nakashima, N.; Hayashida, S.; Yonemori, K. *Chem. Lett.* **1979**, 1416.
(29) Nakashima, N.; Fukushima, H.; Kunitake, T. *Chem. Lett.* **1981**, 1555.

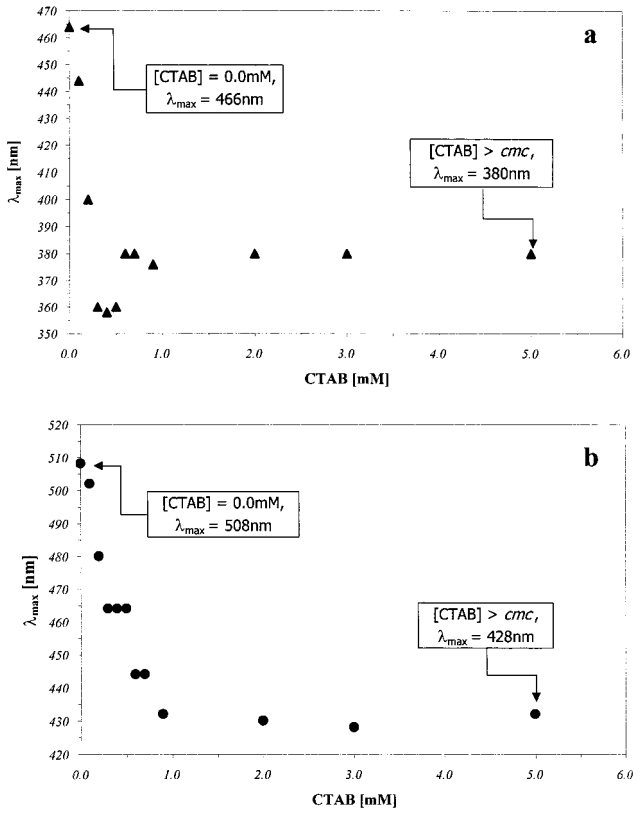

Figure 7. The effect of CTAB concentration on the λ_{max} of entrapped methyl orange in the dried glass (a) and after exposure to air humidity (b).

Table 2. Effects of CTAB on Structural Properties of the Porous Glass

CTAB concn (mM)	SAXS−P(r) before drying I[a] (nm)	II (nm)	I/II[b]	SAXS−P(r) after drying I[a] (nm)	II (nm)	I/II[b]	adsorption data BET[c] (m^2/g)	BJH[d] (Å)	BJH[e] (cc/g)
0.0	13.0			1.4	13.0	4.0	670	<20	0.13
0.2	11.0			1.4	22.4	0.2	610	<20	0.09
0.4	4.5	9.5	1.0	2.1	15.4	0.9	534	<20	0.07
0.8	3.0	9.5	1.3	2.1	14.7	2.1	534	<20	0.08
2.0	3.0	8.5	2.5	2.1	15.0	3.3	554	26	0.13
10.0	3.0			2.8			513	32	0.45

[a] For assignment of peaks I and II, see Figure 9b. [b] Peaks ratio. [c] BET, specific surface area. [d] BJH, average pore diameter. [e] BJH, cumulative pore volume.

scattering behavior for the two extremes, 0.0 and 10.0 mM CTAB, before and after drying, and Table 2 summarizes the results for the other concentrations. As seen in Figure 8, CTAB has a marked effect on the stability of the matrix to drying: While the scattering profile in the absence of CTAB changes greatly upon drying (Figure 8a), the profiles in the presence of the surfactant nearly coincide (Figure 8b). This marked effect is also evident from the distance distribution function (P(r), calculated by the inverse Fourier transform of the scattered intensity). It is seen (Figure 9 and Table 2) that CTAB causes a decrease in the size of the electron density inhomogeneity; that the shape of the distribution function changes from broad (centered at ∼13 nm) to sharp (having its peak at ∼2.5 nm); and that bimodality evolves upon drying for all samples except the one with the highest CTAB concentration. The parallel influence of CTAB on the surface area and porosity of the final, dried monoliths are also summarized in Table 2: It shows a decrease in the surface area from 670 m^2/g at a zero CTAB

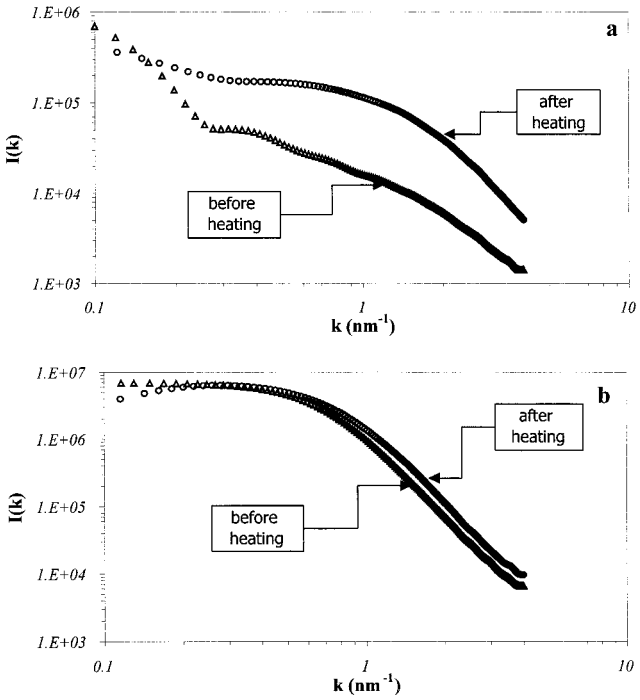

Figure 8. Representative SAXS profiles for the series prepared by procedure 2.2.2 before and after heating (100 °C for 5 h): (a) Sol−gel glass without CTAB and (b) sol−gel glass prepared with 10 mM CTAB.

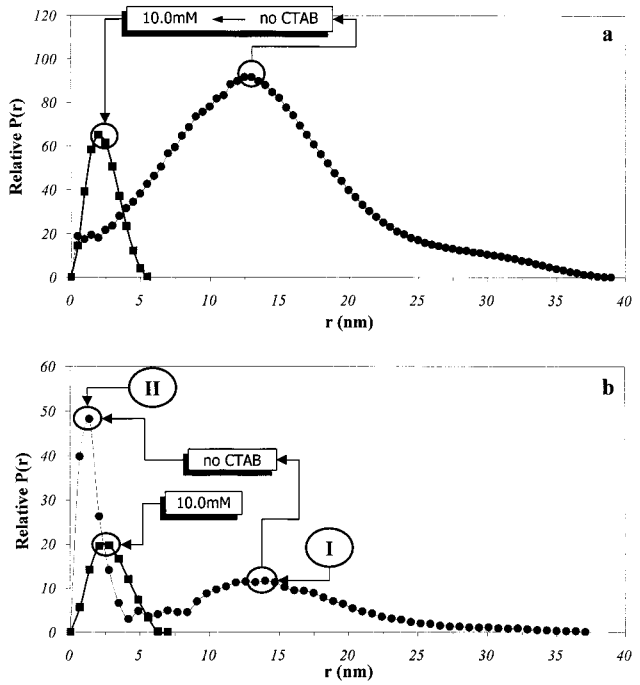

Figure 9. Distance distribution functions, P(r), for the samples of Figure 9: (a) before heating and (b) after heating (100 °C for 5 h).

concentration to 513 m^2/g at 10.0 mM CTAB concentration, accompanied by an increase in the average pore diameter from values bellow 20 nm to a broad distribution around 34 nm. These observations and their relation to the data obtained from the probe molecule, MO, are interpreted and discussed below.

3.3. The Methylated Sol−Gel Matrixes. To strengthen the interpretation we provide below for the possible arrangement of CTAB molecules within the silica cage, we alternatively changed the hydrophobicity of the cage by copolymerizing TMOS with MeTMOS. As shown in Figure 10, this matrix blue-shifted the λ_{max} of MO for the wet glass from the surface-acidic

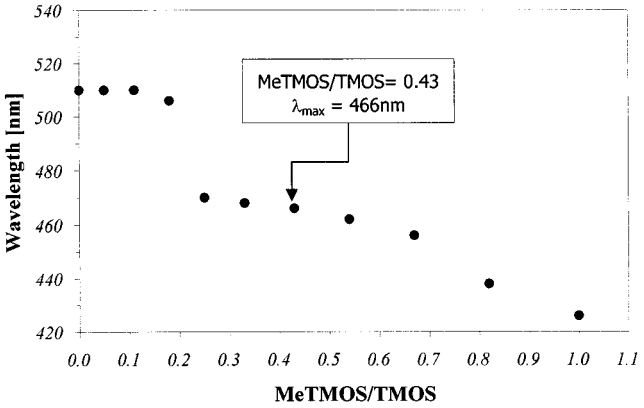

Figure 10. Variations in λ_{max} of methyl orange with the Ormosil composition. (The indicated ratio of 0.43 is used in Figure 11).

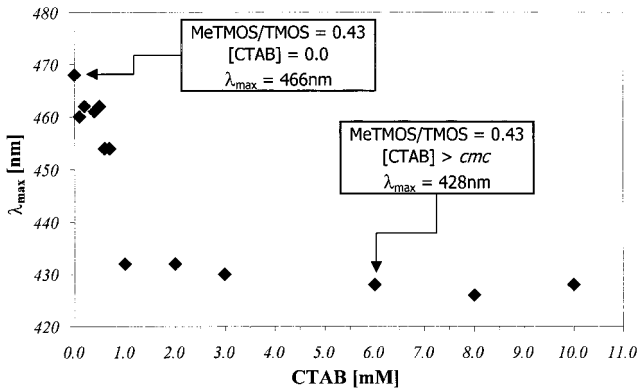

Figure 11. Spectral shifts of methyl orange in the MeTMOS/TMOS = 0.43 Ormosil as a function of CTAB concentration.

510 nm at zero MeTMOS (cf. Figure 7b) to 428 nm for the 50% Me-silica glass. Note the striking resemblance of this value to the value obtained by the micellar environment: MO in this hydrophobic environment "sees" the same environment with entrapped CTAB; that is, it must reside there within a hydrophobic core.

Finally, we tested the effects of changing the CTAB concentration in the environment of an Ormosil, at the MeTMOS/TMOS = 0.43, which, as seen in Figure 11, dictates the anionic form of entrapped MO without imposing hydrophobicity. Indeed, as shown in Figure 11, the increase in CTAB concentration causes again the gradual shift of λ_{max} toward the MO-in-micelle absorption value. The telltale differences in the premicellar zone in all four environments (water, Figure 6; dried sol−gel glass, Figure 7a; wet glass, Figure 7b; and the Ormosil, Figure 10) should be noticed.

4. Discussion

4.1. Introductory Comments. The results summarized in Section 3 point to a new direction in the design of reactive doped sol−gel materials, which we indeed follow in subsequent reports. Thus, on one hand, we have demonstrated once again the general property of doped sol−gel materials: Classical solution chemistry is transferable to the heterogeneous ceramic environment. On the other hand, the new step taken here is to demonstrate that the chemical performance of the dopant can be modified by a careful control of the properties of the cage within which the functional molecule resides.

Since we concentrated here on CTAB as a model co-entrapped modifier, we begin the Discussion by focusing on some of its properties needed to understand the observations. CTAB is a single chained cationic surfactant, the main properties of which, like other surfactants, are derived from its amphiphilic nature. For our purpose, we highlight two of these properties. The first is the ability of the micellar aggregates to grow to many possible variations in shape and form.[31] Thus, CTAB grows anisometrically already around the cmc,[32] and this nonsphericity is a driving force for its directed growth into wormlike or rodlike flexible micelles, resembling a flexible polymer the structure of which is *reversible*.[33,34] An important consequence of this flexibility is the adaptability of the structure to the restrictive shape of the environment, that is, to the pore network of the silica sol−gel matrix.[35] This picture is based also on other observations, such as the recent observation by Anderson et al.[36] that CTAB (like other ionic and nonionic surfactant systems)[37] forms various micellar structures in the sol−gel starting reaction mixture, depending on the co-solvent (methanol) concentration.

The second property is the capability of the silica surface to adsorb CTAB molecules[38] according to the following:

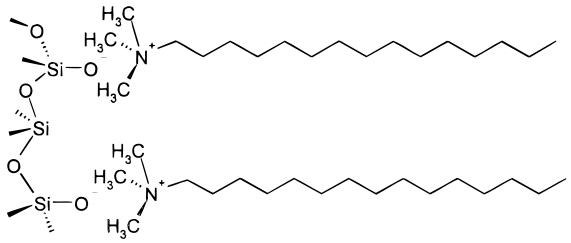

This adsorption, which may take the form of various premicellar structures such as admicelles and hemimicelles,[39] has already been of important use in sol−gel-derived polymers, influencing the sol colloidal stage and the sol to gel transition[40] by homogenizing it and by reducing the internal capillary pressure at the different stages of the porous glass formation. Along the sol to gel to xerogel transitions, an equilibrium exists between micellar-type aggregates of CTAB molecules in the liquid phase and the adsorbed aggregated species, which shifts along the full polymerization process. In the following Discussion sections we show that this picture is in keeping with the experimental observations.

4.2. pK_i and λ_{max} Shifts of the Micellar-Entrapped Indicator in the Sol−Gel Matrix. In this section we interpret the various observed shifts of the entrapped indicators as originating from their specific location within the sol−gel confined micellar phase, and from the movements of the indicators from and to the hydrophobic zones, as their charges change with pH. In analyzing our observations, we also make use of the know-how that has been accumulated in the scientific literature about

(30) Miller, J. M.; Dunn, B.; Valentine, J. S.; Zink, J. I. *J. Non-Cryst. Solids* **1996**, *202*, 279.
(31) Gelbart, W. M.; Ben-Shaul, A. *J. Phys. Chem.* **1996**, *100*, 13169.
(32) Candau, S. J.; Hirsch, E.; Zana, R. *J. Phys. (Paris)* **1983**, *45*, 1263.
(33) Candau, S. J.; Cates, M. E. *J. Phys.: Condens. Matter* **1990**, *2*, 6869, and references therein.
(34) Lin, Z.; Cai, J. J.; Scriven, L. E.; Davis, H. T. *J. Phys. Chem.* **1994**, *98*, 5984.
(35) Ishiwatari, T.; Shimizu, I.; Mitsuishi, M. *Chem. Lett.* **1996**, 33.
(36) Anderson, M. T.; Martin, J. E.; Odinek J. G.; Newcomer, P. P. *Chem. Mater.* **1998**, *10*, 1490.
(37) Matsui, K.; Nakazawa, T.; Morisaki, H. *J. Phys. Chem.* **1991**, *95*, 976.
(38) Iler, R. K. In *The Chemistry of Silica*; Pergamon Press: New York, 1979.
(39) Łajtar, L.; Narkiewicz-Michałek, J.; Rudziński, W.; Partyka, S. *Langmuir* **1994**, *10*, 3754. (b) Fragneto, G.; Thomas, R. K.; Rennie, A. R.; Penfold, J. *Langmuir* **1996**, *12*, 6036.

Table 3. Summary of CTAB Effects on Dopant Properties

family of indicators	direction of pK_i shifts[a]	range of pK_i shifts	$\lvert\Delta\lambda_{max}\rvert = \lambda_{max}^{(g)} - \lambda_{max}^{(s)}$ (low-pH molecular structure)	$\lvert\Delta\lambda_{max}\rvert = \lambda_{max}^{(g)} - \lambda_{max}^{(s)}$ (high-pH molecular structure)
azo dyes (Scheme 1)	$pK_i^{(s)} > pK_i^{(g)}$	$3 \geq \Delta pK_i \geq 0.5$	5 nm $\geq \Delta\lambda_{max} \geq$ 3 nm	40 nm $\geq \Delta\lambda_{max} \geq$ 20 nm
sulfonephthaleins (Scheme 2)	$pK_i^{(s)} > pK_i^{(g)}$	$3.5 \geq \Delta pK_i \geq 0.6$	12 nm $\geq \Delta\lambda_{max} \geq$ 5 nm	20 nm $\geq \Delta\lambda_{max} \geq$ 4 nm
phthaleins (Scheme 3)	$pK_i^{(s)} < pK_i^{(g)}$	$4 \geq \Delta pK_i \geq 2$	colorless	$\Delta\lambda_{max} \pm 5$ nm

[a] g = glass with CTAB; s = solution without CTAB.

the behavior of indicators in surfactant solutions.[41−44] In those sources one finds that the pK_i changes of the indicators result from a combined effect of electrostatic interactions with the surfactant headgroup (Hartley's "sing rule")[41] and the nature of the neutral lipid part and its packing. For each case, we shall propose which parameter is dominant, or which of these parameters work in concert. Of course, each one of the entrapped indicators has its own characteristic behavior and should have been examined separately, but we opted to provide interpretations for the general trends within each family of dyes, as summarized in Table 3.

We begin with the azo-indicators, as represented by MO, the various species of which are shown in Scheme 1. The two main effects observed for this family of dyes were the blue shift in the λ_{max} values in comparison to solution, especially for the basic species, and the pK_i shifts to the acidic range by 1−3 pH units. These shifts can be understood by considering the orientation of the deprotonated species a and the protonated species b−d (Scheme 1) in the micellar environment, as represented graphically in Figure 12 for one MO molecule. The basic form a is oriented fully within the surfactant micellar environment, because the negatively charged sulfonate group of the MO associates with the positive quaternary ammonium group of the CTAB, whereas the noncharged phenylamine residue dissolves in the hydrophobic zone.[22,28,29] Then, with decreasing pH, the azophenylamine moiety becomes positively charged and hydrophilic, resulting in its repulsion from the hydrophobic region to the hydrophilic surroundings of the micellar phase. Indeed, the spectral shifts observed conform to this picture. Species a experiences a hydrophobic environment, which causes a large 10−30 nm blue shift, compared to the dissolution in water and species *d*, which is largely in an acidic water-like hydrophilic environment, shows only a 0−3 nm shift compared to water. The interpretation for the large bathochromic shift obtained for the basic form of MO is corroborated by a conclusion reached by Reeves et al.[45] that the ground state λ_{max} of the MO basic form in water solutions results from the combination of short and long wavelength absorbing species, namely, the nonhydrated a form (Scheme 1) and the azo-hydrated form of a. The pK_i shift to a more acidic value is understood by noticing that, as the pH decreases, the MO moves to a zone in the micellar phase which is densely charged with the positive ammonium ions (Figure 12). This cationic environment associates with the basic moiety of the indicator and buries the azo moiety of MO in the hydrophobic region. As a consequence, a higher concentration of protons is required to reach the azo functional group and the pH needed to reach the pK_i situation is shifted to a higher acidic value. This behavior is shared also by MR and pMR, also azo dyes, showing similar trends in their spectral and indicating ranges (Table 1).

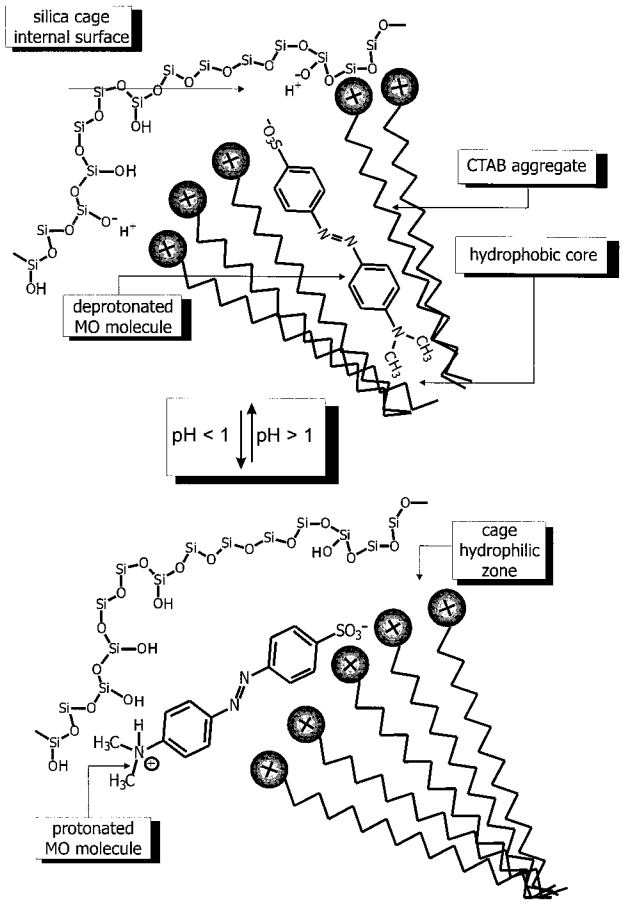

Figure 12. Schematic representation of the relocation of methyl orange (MO) in the sol−gel entrapped micellar environment as a response to pH changes.

The behavior of the leaching profiles of MO (Figure 5) is in agreement with this interpretation: At the lower pH the MO zwitterionic species resides in the water-rich surroundings of the micellar region and is, therefore, relatively accessible for leaching. However, at pH = 2, the singly charged MO molecule resides within the micelle and, protected by the hydrophobicity of this region, is also protected against leaching, with a half-life of several months. The even better leaching behavior of MR at very low pH is ascribed to the close proximity of the negatively charged carboxylate moiety to the positively charged protonated azo group, rendering this molecule more hydrophobic than the MO at the same pH. *The protection against leaching by the micellar environment is a key result of this study.* The appeal of direct, physical entrapment, compared to covalent attachment,[13b] is further strengthened in the context of designing devices for long-term applications by this observation.

Unlike the azo family of indicators, which exhibited marked acidic shifts, the family of the phthaleins (represented by

(40) Jones, S. M.; Friberg, S. E. *J. Non-Cryst. Solids* **1998**, *224*, 249. (b) Mukkamala, R.; Cheung, H. M. *J. Mater. Sci.* **1997**, *32*, 4687. (c) Frieberg, S. E.; Sjöblom, J. In *Industrial Applications of Microemulsions*; Marcel Dekker: New York, Basel, Hong Kong, 1997; p 267.

(41) Fendler, J. H.; Fendler, E. J. In *Catalysis in Micellar and Macromolecular Systems*; Academic Press: New York, 1975.

(42) Healy, T. W.; Lovelock, B.; Grieser, F. In *Solid/Liquid Dispersions*; Academic Press: London, U.K., 1987.

(43) Teisse, J.; Tocanne, J. F.; Pohl, W. G. *Ber. Bunsen-Ges. Phys. Chem.* **1978**, *82*, 875.

(44) Vas, W. L. C.; Nieksch, A.; Jahnig, F. *Eur. J. Biochem.* **1978**, *83*, 299.

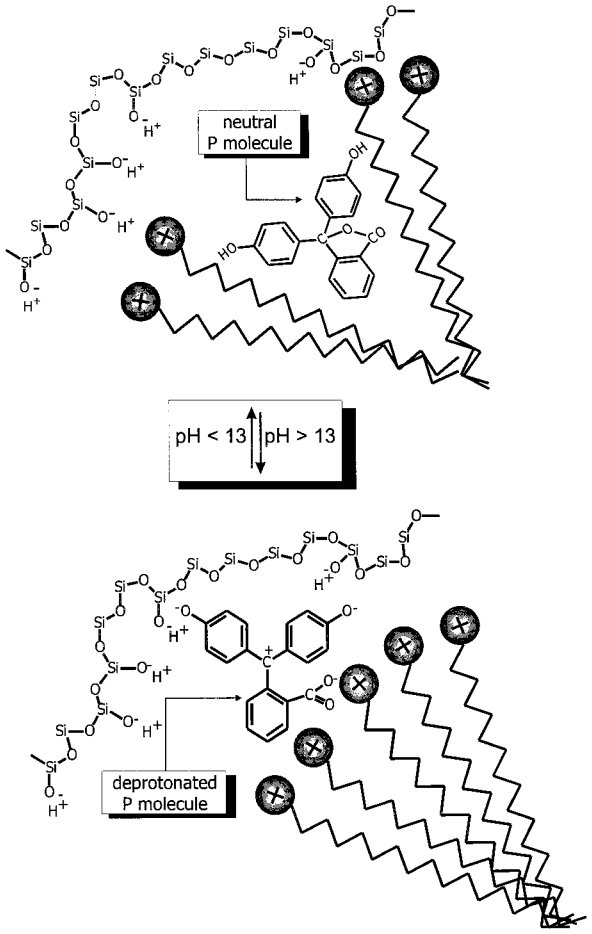

Figure 13. Schematic representation of the relocation of phenolphthalein (P) in the sol−gel entrapped micellar environment as a response to pH changes.

phenolphthalein, P, Scheme 3) experiences a marked *basic* shift in the pK_i value upon entrapment. The main structural difference responsible for this variation is that, opposite of the azo dyes, in the phthaleins, an increase in pH is translated into a transition from a hydrophobic noncharged lactone species (a in Scheme 3) to an anionic hydrophilic one (b and e). The movements within the micellar environment accompanying the changes in the molecular structure of the phenolphthalein indicator are schematically shown in Figure 13. By using this description of the local micellar environment, within which P is localized, we ascribe the higher hydroxyl concentrations needed in order to open the lactone form to the ion-pairing of the hydroxyl anions with the cationic micellar interface. Since P is localized in the hydrophobic zone and the cationic micellar interface forms ion pairs with the anionic hydroxyls, P in its a-protected form must be exposed to higher external pH in order to be affected.

As we have seen in Section 3, particularly interesting results were obtained for the molecules which provide two pH-induced transitions. Our next family of indicators, the sulfonephthaleins (Scheme 2), is one such case because the molecules of this family are indeed capable, in principle, of two protonation/deprotonation steps: From species a to b, and from b to c. As evident from Scheme 2, the increase in pH causes an increase in the number of negative charges, 1, 2, and 3 for species a, b, and c, respectively, and all three species are hydrophilic. They reside, therefore, at the hydrophilic interfacial zone of the silica/micellar phase, and as a consequence, the association strength between the indicator and the positively charged hydrophilic zone of the micelle increases with pH, causing an increase in

Scheme 5. The Amphiphilic Interaction between MO and the CTAB Molecules

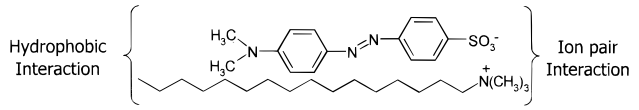

the concentration of the competing protons needed to reach the pK_i. The molecules become then, as the azo dyes, indicators (IN) for higher acidities compared to solution:

$$IN^- \; CTA^+ + H^+ \rightleftharpoons IN{-}H + CTA^+$$

For most of the sulfonephthaleins, only one of the two transitions is seen, namely, the transition from b to c. An interesting example for these single transition cases is that of Cresol Red, which transforms from an indicator for mild bases in solution to an indicator for mild acids in the sol−gel matrix. The two pH transitions of PR and thymol blue are seen as in solution and, following the mechanism suggested above, indeed *both* transitions are seen to be pushed to higher acidities (Figure 3 and Table 1). Again, it should be noted that *negative* pH values become detectable with these two indicators.

The phenomenology of CTAB/sol−gel effects is rich: While in PR and in thymol blue the two indicating ranges are shifted in the same direction, in AL, as we saw (Figure 3), the shifts of the two ranges are in *opposite* directions. This means that it becomes more difficult both to protonate the monoanion b (Scheme 4) into a and to deprotonate it into c. Once again, the location where the various forms of the molecule reside and the pairing of hydroxyls with the positively charged surfactant explain the opposite direction of the two transitions: Thus, unlike the sulfonephthalein zwitterionic species b (Scheme 2), species b of AL is singly charged and the charge is spread out by many resonant structures, two of which are shown in Scheme 4. The monoanion is therefore relatively hydrophobic and buried inside the hydrophobic region of the micellar structure. Higher concentrations of hydronium cations and of hydroxyls are needed therefore to reach it, to form the neutral species a or the dianion c, respectively. And as in the case of P, the higher pH needed for the AL dianion is also due to the competing ion pairing between the interfacial cationic charge and the hydroxyls.

Finally, we wish to comment briefly on the interesting synergistic effect mentioned above and seen in Figure 2, namely, that the combined effect of indicator−micelle interaction with caging in the silica matrix affects the pK_i values stronger than each of these effects alone. As mentioned above, solution studies have shown that the pK_i is affected by the electrostatic interactions and by the packing of the micelle);[41−43] however, of special relevance here is the study of Vas et al.[44] pointing to the importance of the charge *density* in the vicinity of the probe. Thus, the enhancement of these effects in our case would seem to indicate that, within the silica cage, the CTAB molecules are more densely packed, increasing the microscopic amphiphilic nature of the cluster, which in turn, strengthens its effects on the indicator molecule compared to the micellar aqueous solution. Indeed, this proposition is strengthened by several recent reports on the effects of adsorption of surfactants in general[39b,46] and of CTAB in particular[47] onto silica surfaces, which have reached a similar conclusion. In the next Section we are providing some indirect spectral proof for this proposition.

(45) Reeves, R. L.; Kaiser, R. S.; Maggio, M. S.; Sylvestre, E. A.; Lauton, W. H. *Can. J. Chem.* **1973**, *51*, 628.

(46) Kiraly, Z.; Borner, H. K.; Findenegg, G. H. *Langmuir* **1997**, *13*, 3308.

4.3. Concentration-Dependent Aggregation of CTAB within SiO_2 Sol−Gel Glass. As mentioned in Section 3, the relevant observed λ_{max} values of MO are the acidic solution zwitterionic 510 nm peak, the anionic 466 nm maximum in solution (Scheme 1), the 428 nm value of that species within the micelle (Figure 6), and the low (355−380 nm) values at the dried glass. The crucial role of water adsorption in enabling the formation of micellar structures within the sol−gel cages was clearly evident in Figure 7 where, only after environmental humidity adsorption, the micellar 428 nm value was reached. Furthermore, this effect is even seen in the range of the premicellar concentration values in which the λ_{max} drops to as low as 355 nm in the dried glass and never rises above 380 nm (Figure 7a). We attribute these highly blue-shifted values to strong ion-pair/hydrophobic dual interaction as shown in Scheme 5. Thus, by virtue of electrostatic interaction, the positively charged N^+ of CTAB localizes the negative charge on the MO sulfonate moiety, decreasing the weight of resonance structures of species a (Scheme 1); such restriction on resonance is known to cause blue shifts in λ_{max}. It is seen in Figure 7a (the dried glass) that the interaction of MO with the bare silica (466 nm) is replaced quite fast with the ion-paired interaction and that these ion-paired species prevail at all higher CTAB concentrations (Figure 7a). They seem to be the tightest (355 nm) at a CTAB concentration of 0.4 mM. Along the lines of the thermotropic behavior observed by Ogawa et al.[48] for cetyltrimethylammoniumchloride (CTAC) in a silica matrix (as probed by pyrene fluorescence), we associate the blue shift to 380 nm with an increase in the local hydrophobicity around the MO indicator which, in turn, results from the increased microviscosity of the micellar phase due to the drying of the matrix. We also draw attention again to the observation that the fully dried silica is a quite poor proton-donating species: The zwitterionic form of MO (508 nm, Figure 7b) is observed only under humid conditions, and the dried glass forces MO to be in its anionic form (466 nm, Figure 7a). This demonstrates that the role of drying on the properties of the cage of the silica must not be underestimated.

The interpretation that the 428 nm of MO in the CTAB/sol−gel matrix results from a hydrophobic environment was nicely proven by the experimental results obtained with MeTMOS: A sol−gel matrix, prepared from MeTMOS/TMOS = 1:1, gives for MO in a cage rich with methyl groups the same 428 nm value (Figure 10). In fact, one can divide Figure 10 into two regions: the 510−466 nm region (molar ratios 0−0.43 respectively), which represents mainly the increase in the blocking of the silanol proton donation ability to MO, up to the point where the concentration of the zwitterionic form is too small to be detected and only the basic form prevails; and the 466−428 nm region (molar ratios 0.43−1.0, respectively) in which MO is only in the anionic form, and thus the shift is accounted for by the increase in hydrophobicity alone.

In parallel to probing the micellar CTAB environment with MO, it was interesting to determine the effects of the changes in the surfactant low concentrations on the materials microscopic structure[17] by SAXS and BET measurements. The most practical observation that the SAXS measurements revealed is that, at a CTAB concentration of 10.0 mM, the matrix becomes stable to low-heat treatment (Figure 8). It is of practical importance because it is known that final xerogels continue to "work" for many months. This becomes a problem when one wishes to commercialize sol−gel-based devices and products. It now seems that addition of CTAB can help solve this problem. The fact that the sharp peaks in the P(r) profiles (Figure 9 and Table 2) before and after heating nearly coincide helps to interpret the appearance of the bimodality in the presence of lower CTAB concentration: It is evident from Figure 9 that CTAB is responsible for the ∼2.5 nm smaller mode and to the transition of the population from the wide size inhomogeneity into this small size upon heating. The role of CTAB in forming the small size electron density inhomogeneities is related to its function as a homogenizing tool in the polymerization mixture, by forming a narrow distribution of the dense silica building-block particles.[5,6] The wider distributions of P(r) observed without and at low concentrations of CTAB correlate with the higher surface areas and with smaller average pore sizes (Table 2). This may be attributed to an open, less dense packing of the basic particles, compared to a more closely packed arrangement at the 10 mM CTAB (Table 2) due to an increase in the population of the CTAB micellar structures at higher surfactant concentrations. These observations are in keeping with the set of principles set up recently by Muthukumar et al.,[49] which pointed to the effects of changing interfacial tension (by changing surfactant concentration) on the spontaneous selection of primary length scales in polymerization.

5. Conclusion

Sol−gel materials provide a new way to study the surface-active agent concentration effects on probe molecules, which was not possible in solution: In solution one has sharp transitions between the surfactant monomer and its several possible aggregated forms, such as the classical micelle; within the sol−gel matrix, such transitions appear to develop in a continuous mode. Thus, on one hand we found conditions for having CTAB within the matrix in an isolated, adsorbed form; then, going gradually through more and more pronounced aggregation displaying distinct hydrophobic and hydrophilic regions, we ended in conditions where the micellar structure of the entrapped CTAB is fully evident.

We have shown here that the co-entrapment of a surfactant with dopant molecules within sol−gel matrixes is a convenient way to modify cage properties and, therefore, the dopant properties and the specific functionality of these materials. As we shall show in subsequent reports, this is a general methodology. We believe that, as much as nonpolymerizable substituents on the monomer proved to be very successful and are widely used in tailoring material functionality, the horizon waiting for surfactants in this sense is no less exciting.

Acknowledgment. We thank the Israel Ministry of Science and Arts for a Special Infrastructure Fund (Tashtiot), the Israel Science Foundation, and the German-Israel Science Foundation (GIF) for supporting this study.

JA991269P

(47) Adamczyk, Z.; Patra, G.; Karwiński, A. *Tenside, Surfactants, Deterg.* **1998**, *4*, 261.

(48) Ogawa, M.; Igarashi, T.; Kuroda, K. *Chem. Mater.* **1998**, *10*, 1382.

(49) Muthukumar, M.; Ober, C. K.; Thomas, E. L. *Science* **1997**, *277*, 1225.